XLIII CILAMCE
21–25, November, 2022
FOZ DO IGUAÇU – PR – BRAZIL

DESIGN OF INJECTOR PLATES FOR HYBRID ROCKET MOTORS TEST BENCH WITH GASEOUS OXYGEN

Paulo Gabriel Cunha Martins[1], Kesiany Máxima de Souza[2], Rene Gonçalves[3], Leonardo Henrique Gouvêa[1], Cristiane Aparecida Martins[1]

[1]*Dept. of Propulsion, Instituto Tecnológico de Aeronáutica*
[2]*Dept. of Energy, Instituto Tecnológico de Aeronáutica*
[3]*Dept. of Chemistry, Instituto Tecnológico de Aeronáutica*
[1−4]*Praça Marechal Eduardo Gomes, 50 - Vila das Acacias, São José dos Campos - SP, 12228-900, Brazil*
paulomartins92@gmail.com, kesianymaxima@gmail.com, renefbg@ita.br, gouvea@ita.br, cmartins@ita.br

Abstract. Hybrid rocket motors have been intensively studied in universities because of their many advantages compared to other chemical rocket motors. They are safe, simple to handle, present low cost, environmental cleanliness, and throttling features. Because of these reasons, hybrid motors injection plate is a primary item. There is a lot of available experimental data about the atomization of particles for liquid injection. However, for laboratory applications, in which liquid oxygen is more expensive and challenging gaseous oxygen is desirable. From this point of view, the present study is motivated by the lack of literature about injection plates for compressible fluids. This paper presents an analytical and numerical design of injectors for gaseous oxygen. In the analytical study section, continuity, ideal gas, and atomization equations present in literature have been used to design a showerhead injection plate for the desired pressure drop. The numerical study made it possible to model a viscous flow through the designed injection plate, resulting in slightly higher pressure drops than isentropic analytical results since the theoretical results do not account for viscous losses. This numerical model validation enabled the design of more complex injection plates, such as hollow-cone, pressure-swirl, and vortex ones.

Keywords: Injector plates, Gaseous oxygen injection, Compressible flow, Cold flow simulation, k-ω SST turbulence model

1 Introduction

Nowadays, hybrid rocket propulsion has been the preferable option to be studied in universities since it is safer, cheaper, and less complex than solid and liquid rocket propulsion. Moreover, it offers a wide range of research, such as structural analysis, combustion analysis, gas dynamics, control systems, et cetera. The work presented is a part of the design of a hybrid rocket motor of 100 N designed by [1], that nowadays is active at LTF in ITA. The objective of this paper is to show the methodology applied in the injector plate design for compressible gaseous oxygen and go through step by step.

The first step starts with the analytical procedures presented in section 2, which relates the mass flow rate equation with the total-to-static pressure ratio equation of compressible flows. Right after, an experimental-based correlation is presented. This correlation calculates the discharge coefficient knowing only the geometry and the flow properties, such as its kinematic viscosity, Reynolds number, and the orifice-length to diameter ratio. Some of these data were retrieved from NIST [2] and others were assumed following a suggestion from Humble et al. [3], such as the pressure drop through the injector orifices. After this analytical methodology, it was possible to correlate the number of orifices to their diameter and the pressure loss, resulting in an initial guess of the injector plate geometry.

Figure 1 presents the four kinds of injectors designed. The objective is to guide the oxidizer flow into different path lines during the tests. With that, it is expected other opportunities to study the influence of the oxygen jets on the regression rate of the fuel and pressure drop in the oxidizer line. The axial injector was designed analytically and numerically, and the other three were designed only numerically due to their complex geometries. These four types of injectors were studied experimentally by Bouziane et al. [4] for the liquid nitrous oxidizer injection. It was observed that the Swirl type 1 presents a higher regression rate compared to the others, followed by the conical, axial, and swirl type 2. On the other hand, the conical one presents the worst efficiency compared to the others. The authors suggest that it can be because of the relatively large amount of grain chunks exhausting the nozzle due to the poor mechanical properties of the paraffin, while the swirl type 1 and 2 show efficiency in the specific impulse of around 78%.

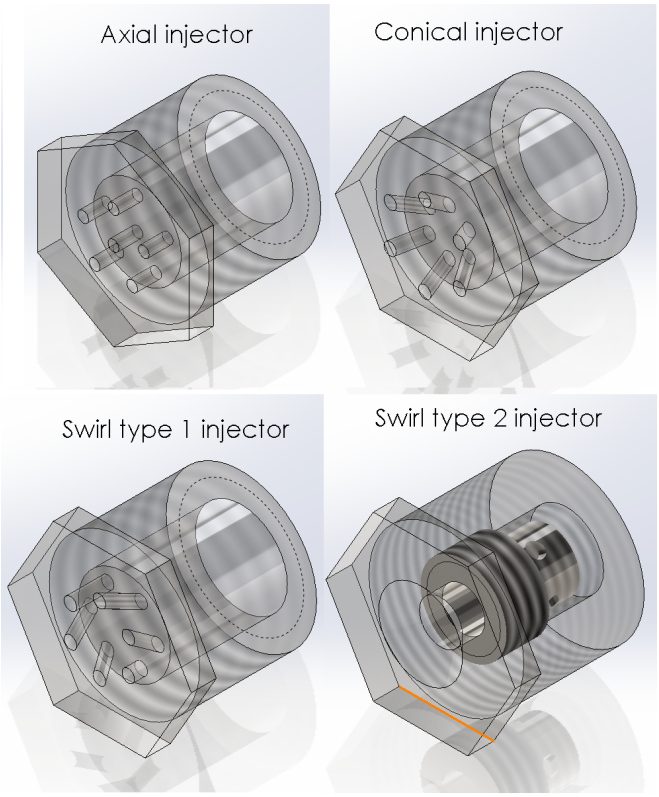

Figure 1. Injectors CAD characteristics.

The numerical simulations are the second step of the design and are presented in section 3. There show the control volume, boundary conditions, and the mesh for each one of the injectors. These injector plates were designed to be used with gaseous oxygen in a hybrid rocket motor combustion chamber. The combustion chamber is composed of three orifices equally spaced and it is presented in section 3, where it shows the flow pathlines inside of them.

2 Governing Equations

To model an injector plate for a compressible fluid such as gaseous oxygen, Eqs. 1 and 2 from Hill and Peterson [5] and Yahya [6] were employed. They describe the mass flow rate and total to a static pressure ratio of a compressible flow, respectively, where $\dot{m}$ is the mass flow rate, A area, P_0 total pressure, T_0 total temperature, γ heat capacity ratio, R specific gas constant, M Mach number, and P static pressure.

$$\dot{m} = \frac{AP_0}{\sqrt{T_0}}\sqrt{\frac{\gamma}{R}}M\left[1+\frac{\gamma-1}{2}M^2\right]^{-\frac{\gamma+1}{2(\gamma-1)}} \tag{1}$$

$$\frac{P_0}{P} = \left(1+\frac{\gamma-1}{2}M^2\right)^{\frac{\gamma}{\gamma-1}} \tag{2}$$

However, equation 1 accounts for an isentropic, and ideal gas flow. As so, a discharge coefficient C_D must be considered as described by Lefebvre and McDonell [7] to account for pressure losses and wall detachment. It is related to the experimental mass flow rate by equation 3.

$$\dot{m}_{exp} = C_D\frac{AP_0}{\sqrt{T_0}}\sqrt{\frac{\gamma}{R}}M\left[1+\frac{\gamma-1}{2}M^2\right]^{-\frac{\gamma+1}{2(\gamma-1)}} \tag{3}$$

As suggested by Asihmin et al. [8], the calculation of discharge coefficient can be done by equation 4, for an orifice-length to diameter ratio l_o/d_o in the range $2-5$ and Reynolds number R_e from 100 to $1.5x10^5$. R_e can be determined from equation 5 and 6.

$$C_D = \left[1.23+\frac{58(l_o/d_o)}{R_e}\right]^{-1} \tag{4}$$

$$Re = \frac{\rho v d_o}{\nu} \tag{5}$$

$$v = \frac{\dot{m}}{N_{inj}\rho A} \tag{6}$$

Table 1 presents the fluid and geometric properties of a gaseous oxygen injector. The thermodynamic properties were retrieved from NIST [2] at a temperature of 298 K and pressure of 10 bar.

Table 1. Properties of gaseous oxygen injection.

$\dot{m}[g/s]$	$l_o[mm]$	$\rho[kg/m^3]$	$\nu[Pa\cdot s]$
25	3	24.698	2.086110^{-5}
$R[J/kgK]$	γ	$T_0[K]$	$P[Pa]$
254.4219	1.4314	298	10^5

As suggested by Humble et al. [3], the pressure drops Δp across an injector plate must be approximately 30% of the chamber pressure in order to ensure stability. As the present motor design has a chamber pressure of 10 bar, Δp across the injector must be higher than 3 bars. Accounting for a Δp = 5 bar, we have that $P_0/P = 15/10 = 1.5$, which applying Eq. 2 gives a Mach number at the injector orifice of 0.78. With these values, equation 4 can be solved for a various number of injector orifices N_{inj}. Figure 2 shows these results for different orifice diameters.

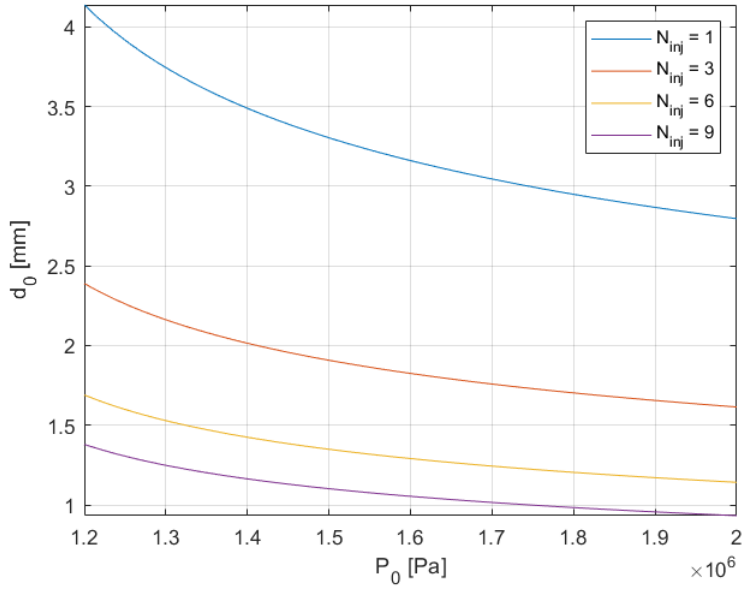

Figure 2. Orifice diameter relation with total pressure and injectors quantity.

For $N_{inj} = 6$, and a pressure drop of $P_0 - P = 5$ bars, which requires an orifice diameter of $d_o = 1.35$, the orifice length to diameter ratio l_o/d_o is 2.22, and Re number is $1.13x10^5$. These values are inside the ranges researched by Asihmin et al. [8] for discharge coefficient analysis, so equation 4 can be correctly applied. Finally, the designed injection plate have the properties shown at table 1.

Table 2. Properties of the axial injector plate designed.

N_{inj}	$d_o[mm]$	$\Delta p[bar]$	$Mach$
6	1.35	5	0.78

3 Numerical Modeling

Previous analytical modeling could be applied only for the axial injector design. As so, the four injectors were numerically modeled by using the software *Ansys Fluent*®, where the analytically results from the axial injector design were applied to validate the simulations. The injector plate was designed for a hybrid rocket motor with gaseous oxygen and a PMMA grain with three combustion chambers. Past simulations that contributed to the configurations of this one presented here are available at [9] and at [10]

3.1 Mesh

The simulations were carried out with the mesh and contour conditions shown in Figs. 3, 4, and 5. The control volume accounts for an oxygen inlet, the injection plate, a pre-chamber, and a part of all three combustion chambers. The meshes have 2811665, 3061371, 3169794, and 3209397 elements for the axial, swirl 1, swirl 2, and the conical injector, respectively.

Care was taken to refine the mesh in the critical regions where high gradients of velocity are expected, such as at the injector plate and near the walls, as can be better observed in Fig. 5. Also, the region near the combustion chambers inlet was refined to better capture the flow entering them.

The meshes differed only on the injector plate, as shown in figure 4.

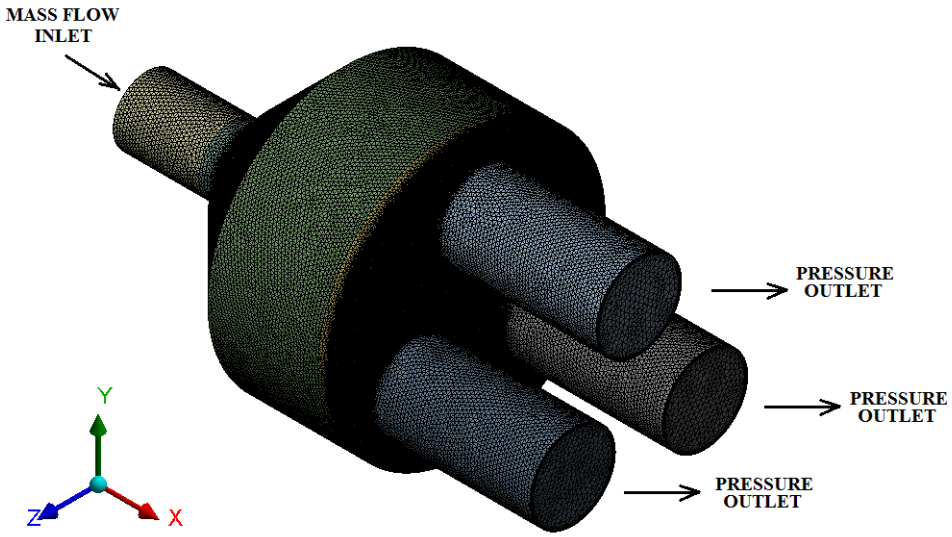

Figure 3. External mesh and boundary conditions for the overall injector simulations.

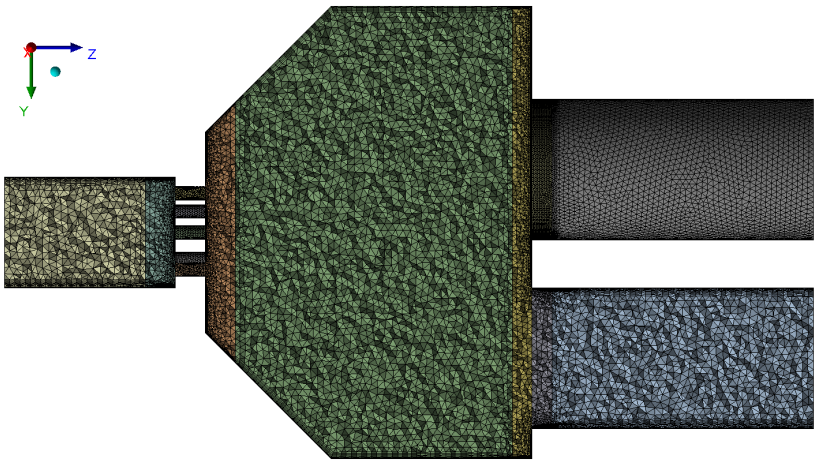

Figure 4. Internal mesh for the overall injector simulations.

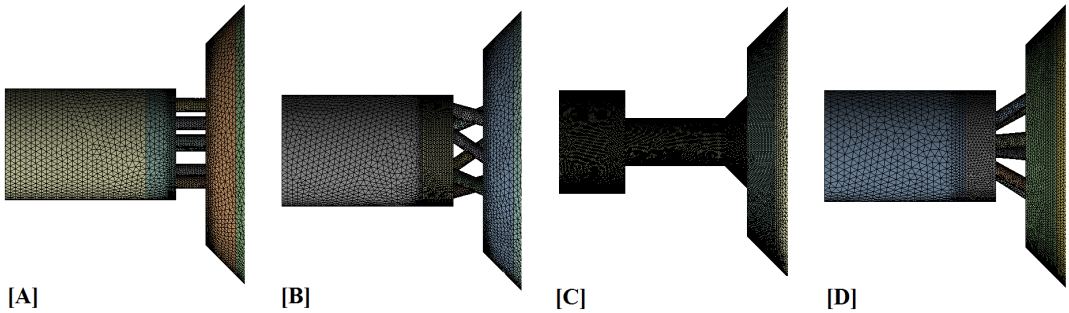

Figure 5. Mesh detail of the [A] axial, [B] swirl 1, [C] swirl 2, and [D] conical injector plate.

3.2 Setup

The models applied to the numerical study are shown in Tab. 3. The numerical flow modeling in the simulations presented is based on the solution of the $RANS$ (Reynolds-Averaged Navier-Stokes) equations for turbulent fluids. In *Fluent*, these governing equations are discretized into finite volumes and then solved by algebraic approximations or differential equations, as explained by Ahmed et al. [11]. The solver is pressure-based since an overall low velocity is expected, and no shock waves must be formed. Moreover, to save computational costs, the regime was considered a steady-state.

The turbulence model chosen is the k-ω SST model from Menter [12]. This model allows using a less refined mesh without losing quality in the results, as explained by Menter et al. [13]. It is a low Reynolds model and has two functions: near the wall, it calculates the properties of the fluid more precisely using the standard k-ω model from Wilcox [14], and in the core of the fluid, it uses the k-ϵ model, which results in the best performance of both models.

A coupled scheme was applied to solve the flow problem since it results in a robust and efficient solution for a steady-state flow with a single phase. Finally, a second-order upwind scheme was applied for spatial discretization of density, momentum, turbulent kinetic energy, specific dissipation rate, and energy equations, whereas the pressure interpolation is also of second order.

Table 3. Models applied to the numerical study.

Solver	Pressure-based
Regime	Steady-state
Turbulence	SST k-ω
Scheme	Coupled
Spatial Discretization	2nd order upwind
Pressure Interpolation	2nd order

3.3 Results

Tab. 4 shows some results from the numerical study. The pressure drop between the inlet and outlet is 5.4 $bars$, very close to the axial injector modeled analytically for a pressure drop of 5 $bars$. However, these higher pressure drop previewed numerically must be a consequence of the higher pressure losses modeled, caused by viscous forces and turbulence. The other three injectors were then numerically modeled to present a pressure drop of nearly 5 $bars$. The minimum temperature values are at the injector orifices, where the Mach number is maximum, although it is not high enough for the flow to be shocked.

Table 4. General results from the numerical study.

Injector	$P_{inlet}[bar]$	$P_{outlet}[bar]$	y^+_{max}	$T_{min}[K]$	$Mach_{max}$
Axial	15.4	10	194.4	257.6	0.92
Swirl 1	15.7	10	201.37	252.27	0.95
Swirl 2	15.4	10	96.09	255.3	0.91
Conical	15.8	10	224.7	252.3	0.95

The maximum value of y^+ at the walls was examined for all meshes. The values are lower than 300 as shown in Tab. 4, which must satisfy the law-of-the-wall as suggested by Sutalo [15]. Following [13], there is no problem to get y^+ values far from the unit due to the capacity of the model to predict this distance and to use a wall function in the logarithmic region. For less accurate meshes with $y^+ > 1$ an error of 2% in the calculation of the wall shear stress.

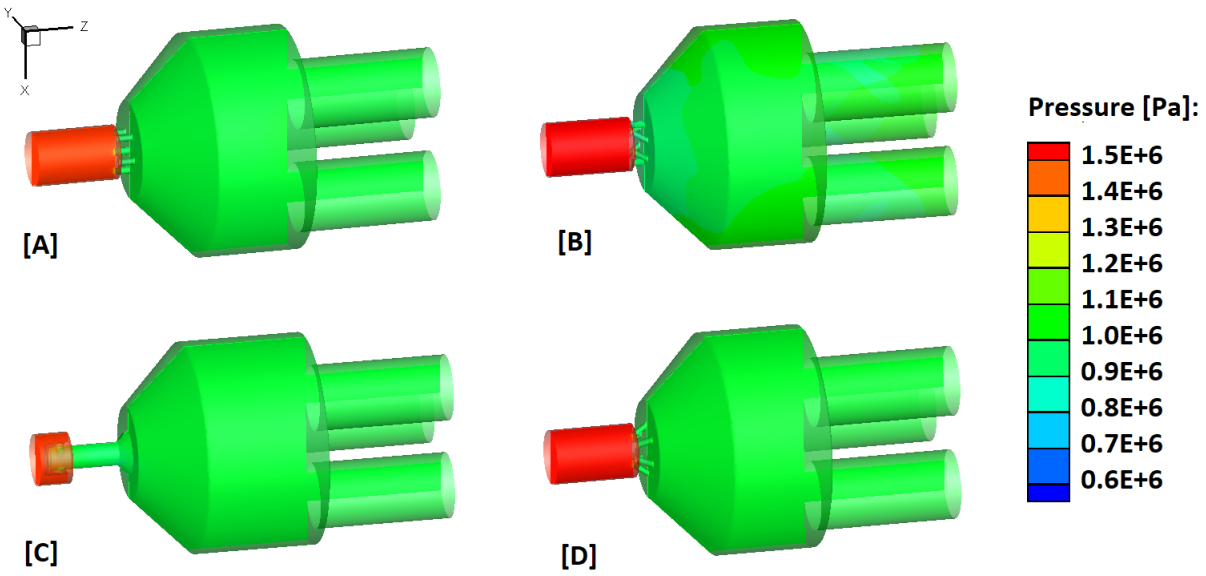

Figure 6. Pressure contours of the [A] axial, [B] swirl 1, [C] swirl 2, and [D] conical injector plate.

Figure 6 shows the contours of pressure within the control volumes, which make it possible to visualize the pressure drop across the injector plates. In [A], the pressure drop across the axial injection plate is approximately 5 bars, as calculated before. The other injection plates were designed also to have nearly this pressure drop to, as explained previously, ensure stability.

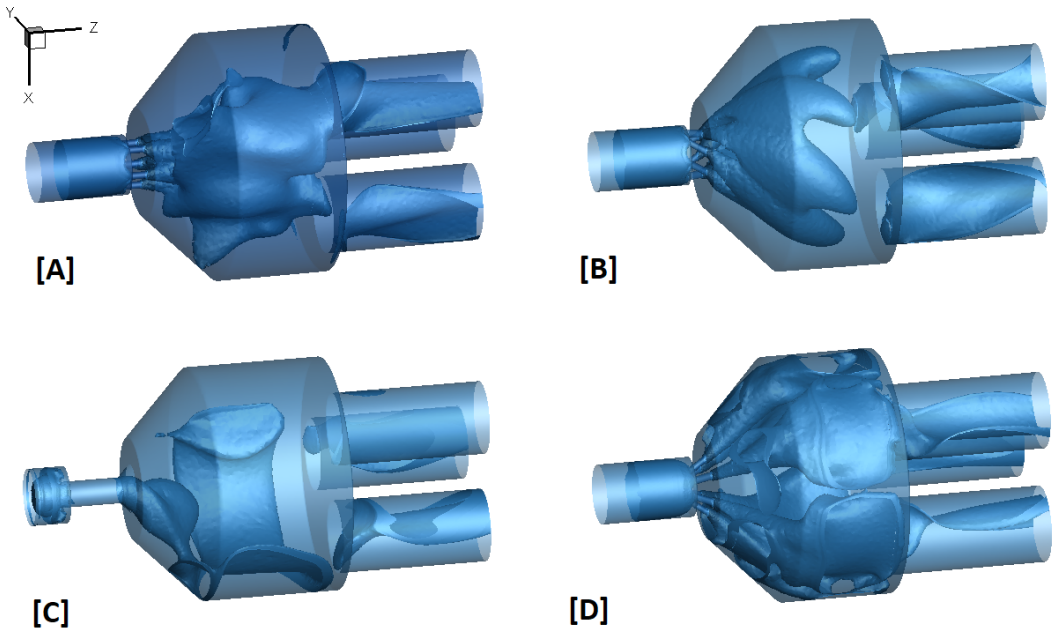

Figure 7. Iso-surface of $10m/s$ axial velocity in the [A] axial, [B] swirl 1, [C] swirl 2, and [D] conical injection control volume.

Figure 7 shows the iso-surface for an axial velocity of $10m/s$ in the overall injectors. These plots allow observing the 3-D fluid behavior inside the pre-chamber. Comparing the results of the axial injector with the others in the pre-chamber before the combustion chambers, it is noted that the swirl 1 shows a well-predetermined path-line with an axial and a radial swirl direction, the swirl type 2 looks like it is pointed to the wall with a swirl

direction and the flow is touching the walls, and the conical one is as well pointed to the walls but without the swirl direction. Analyzing the combustion chambers all the flows enter the holes with a swirl-type path-line.

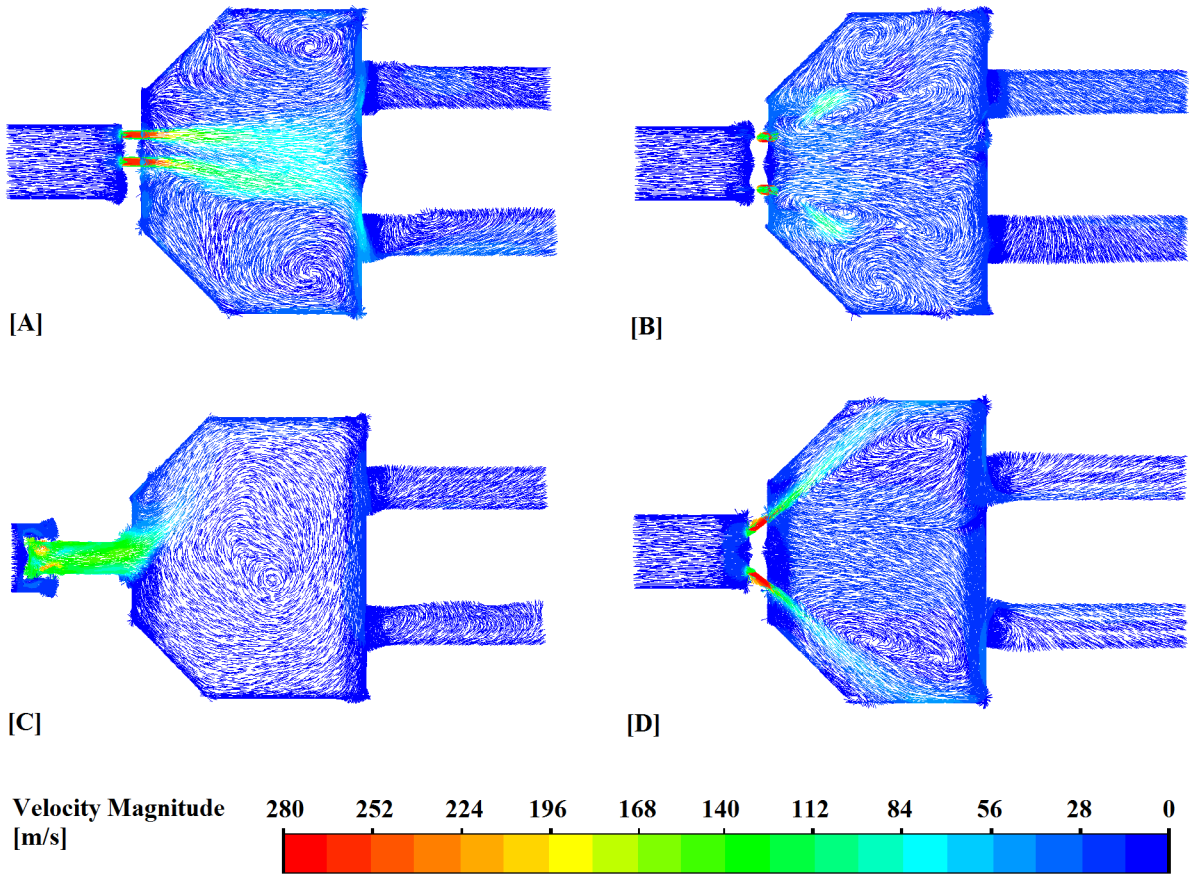

Figure 8. Vector contour in a central plane of the [A] axial, [B] swirl 1, [C] swirl 2, and [D] conical injection control volume.

Figure 8 shows the velocity-vector contour for all injector simulations. It allows observing the vortices formed inside the pre-chamber. At a central plane, the axial injector builds two large vortices. The swirl 1 injector generates at least six small vortices. Swirl 2 generates a single large vortex around all the chamber, and the conical injector results also in two large vortices, but in the opposite direction of the axial injector vortices.

4 Conclusions

This work developed an analytical methodology to design an axial injector plate to flow gaseous oxygen in a hybrid rocket motor. Compressible flow equations for real gases were used in order to get better accuracy in the design. This analysis was validated with a simulation performed in Ansys fluent considering as control volume the 3D geometry upstream and downstream the injector plates until the beginning of a three combustion chambers hybrid rocket motor.

The simulations showed a slight deviation of 0.4 bar from the analytical calculation, which was believed to be caused by the viscous forces and turbulence considered in the numerical study. The simulation methodology based on the pressure drop through the axial injector plate was proven to be validated based on the result obtained. The same simulation methodology was applied to the other injectors' configurations. The injector swirl 1 showed better efficiency in generating vortexes inside the pre-chamber compared to the others. All the results shown numerically here must be further studied experimentally to validate the pressure drop through the injector plates and hence the simulation methodology.

Acknowledgements. My thanks to CAPES for their financial support. The authors would like to acknowledge the financial support of ITAEx (project number 192027) and CNPq (project numbers 428039/2018-9, 432410/2018-0, and 406726/2018-3).

Authorship statement.

The authors hereby confirm that they are the solely liable persons responsible for the authorship of this work and that all material that has been herein included as part of the present paper is either the property (and authorship) of the authors or has the permission of the owners to be included here.

References

[1] P. G. C. Martins. Design of a paraffin/gox lab-scale hybrid rocket motor. Master's thesis, Aeronautics Institute of Technology, São José dos Campos, 2018.

[2] NIST. Chemistry webbook - isothermal properties for oxygen fluid data. retrieved 10 May 2019 from https://webbook.nist.gov/chemistry/fluid/, 2019.

[3] R. W. Humble, G. N. Henry, and W. J. Larson. *Space Propulsion Analysis and Design*. McGraw-Hill Companies,Incorporated, 1995.

[4] M. Bouziane, A. E. Bertoldi, P. Milova, P. Hendrick, and M. Lefebvre. Performance comparison of oxidizer injectors in a 1-kn paraffin-fueled hybrid rocket motor. *Aerospace Science and Technology*, vol. 89, pp. 392–406, 2019.

[5] P. Hill and C. Peterson. *Mechanics and Thermodynamics of Propulsion*. Pearson Education, MA, United States, 2nd edition, 1992.

[6] S. M. Yahya. *Fundamentals of Compressible Flow with Aircraft anf Rocket Propulsion*. New Age International Publishers, 3rd edition, 2006.

[7] A. H. Lefebvre and V. G. McDonell. *Atomization and Sprays*. CRC Press, FL, United States, 2nd edition, 2017.

[8] V. Asihmin, Z. Geller, and Y. Skobel'cyn. Discharge of a real fluid from cylindrical orifices (in russian). *Oil Ind.*, vol. 9, 1961.

[9] P. G. C. Martins and O. Shynkarenko. Flow Analysis Inside the Combustion Chamber and the Nozzle of a Hybrid Rocket Motor. *25th International Congress of Mechanical Engineering*, pp. COB–2017–0990, 2017.

[10] P. G. C. Martins, de K. M. Souza, and de M. Lemos. Numerical Study of Rugosity Effects in a Sinusoidal Pipe by Apllying k-Omega SST Turbulence Model. *25th International Congress of Mechanical Engineering*, pp. COB–2019–0963, 2019.

[11] G. Ahmed, A. Abdelkader, A. Bounif, and I. Gokalp. Reduced chemical kinetic mechanisms: Simulation of turbulent non-premixed ch_4-air flame. *Jordan Journal of Mechanical and Industrial Engineering*, vol. 8, n. 2, pp. 66–74, 2014.

[12] F. R. Menter. Two-equation eddy-viscosity turbulence models for engineering applications. *AIAA Journal*, vol. 32, n. 8, pp. 1598–1605, 1994.

[13] F. R. Menter, M. Kuntz, and R. Langtry. Ten Years of Industrial Experience with the SST Turbulence Model. *Turbulence Heat and Mass Transfer 4*, vol. 4, pp. 625–632, 2003.

[14] D. Wilcox. *Turbulence modeling for CFD*. DCW Industries, Incorporated, 1993.

[15] F. Sutalo. Evaluation of variants of enhanced wall treatment wall function in turbulent flow simulations. Master's thesis, University of Zagreb, Zagreb, 2017.